PROCEEDINGS OF SPIE

SPIEDigitalLibrary.org/conference-proceedings-of-spie

Residual wavefront control of segmented mirror telescopes

Sam Ragland, Peter Wizinowich, Maaike van Kooten, Michael Bottom, Ben Calvin, et al.

Sam Ragland, Peter Wizinowich, Maaike van Kooten, Michael Bottom, Ben Calvin, Michael Fitzgerald, Philip Hinz, Rebecca Jensen-Clem, Dimitri Mawet, Eliad Peretz, "Residual wavefront control of segmented mirror telescopes," Proc. SPIE 12185, Adaptive Optics Systems VIII, 121850Y (29 August 2022); doi: 10.1117/12.2630269

SPIE.

Event: SPIE Astronomical Telescopes + Instrumentation, 2022, Montréal, Québec, Canada

Residual Wavefront Control of Segmented Mirror Telescopes

Sam Ragland[1*], Peter Wizinowich[1], Maaike van Kooten[2], Michael Bottom[3], Ben Cavin[4], Michael Fitzgerald[4], Philip Hinz[2], Rebecca Jensen-Clem[2], Dimitri Mawet[5], Eliad Peretz[6]
[1]W. M. Keck Observatory, Kamuela, Hawaii, USA; [2]Univ. of California, Santa Cruz, USA; [3]Institute for Astronomy, University of Hawaii at Hilo, USA; [4]University of California, Los Angeles, USA; [5]Department of Astronomy, California Institute of Technology, USA & Jet Propulsion Laboratory, California Institute of Technology, USA; [6]NASA Goddard Space Flight Ctr. (United States)
*sragland@keck.hawaii.edu

ABSTRACT

Uncorrected residual wavefront errors limit the ultimate performance of adaptive optics (AO) systems. We present different contributing factors and techniques to estimate and compensate these wavefront errors in the Keck natural guide star (NGS) AO systems. The error terms include low order static and semi-static aberrations from multiple sources, periodic and random segment piston errors, single-segment low order aberrations, wavefront sensor aliasing, vibrations, calibration drifts, and AO-to-telescope offload related errors.

We present the design of a new AO subsystem, a residual wavefront controller (rWFC) to monitor the performance of the AO control loops and the image quality of the AO science instruments and apply the necessary changes to the telescope and AO parameters to minimize the residual wavefront errors. The distributed system consists of components at the telescope, AO bench and the science instruments. A few components of this system are already tested as on-demand stand-alone tools and will be integrated into a high-level graphical user interface (GUI) to operate the system. The software tool will periodically collect AO telemetry data, perform control loop parameter optimization and update AO parameters such as loop gains, centroid gain, etc. In addition, the system will analyze the science data at the end of each exposure and estimate telescope/AO performance when a bright point source is available in the science field.

The benefits of reducing or eliminating the residual wavefront errors have broad implications for optical astronomy. Testing these techniques on a segmented telescope will be extremely useful to the teams developing high contrast AO systems for all extremely large telescopes and future segmented space telescopes.

Keywords: telescope phasing, segment piston errors, residual wavefront errors, low order static aberrations, high contrast imaging, vibration.

1. INTRODUCTION

W. M. Keck Observatory (WMKO) was the first to implement both natural guide star (NGS) and laser guide star (LGS) AO systems on a large telescope [1][2] to achieve angular resolutions in the near-infrared that match the capabilities of the Hubble Space Telescope in the visible. WMKO has endeavored to continually improve the capabilities of the Keck adaptive optics (AO) systems. One such effort is understanding and addressing the observed residual wavefront errors from the telescope and the AO system [3][4].

The Keck telescopes are the first large aperture optical telescopes to successfully implement segmented mirror technology [5]. The segments are phased, using a phasing camera [6][7], to provide diffraction-limited images with AO-fed instruments in the near-infrared. The success of the Keck telescopes provided a basis for the development of other large aperture telescopes, such as the Hobby-Eberly Telescope (HET), Southern African Large Telescope (SALT), Gran Telescopio Canarias (GTC), Large Sky Area Multi-Object Fiber Spectroscopic Telescope (LAMOST), and James Webb Space Telescope (JWST). Segmented mirror technology has also been adopted as the path forward to building the next generation of extremely large telescopes such as the Thirty Meter Telescope (TMT), and European Extremely Large Telescope (ELT).

The broad questions asked in this paper is whether the first-generation segmented mirror technology and the adaptive optics are ready to: (1) take on the challenges of high contrast imaging to characterize habitable zone exoplanets, (2) enable visible AO science, and (3) fully benefit from recent extreme AO developments.

Adaptive Optics Systems VIII, edited by Laura Schreiber, Dirk Schmidt, Elise Vernet,
Proc. of SPIE Vol. 12185, 121850Y · © 2022 SPIE
0277-786X · doi: 10.1117/12.2630269

To take on these questions, we review the error budget of the Keck AO systems and explore ways to measure and correct residual wavefront aberrations that exist in the optical system, including the telescope, AO system, and the science instrument. The effects primarily responsible for the residual aberration in the AO system include (1) residual low order aberrations in the system due to optical effects and calibration limitations, (2) systematic bias in the phasing of the segments of a large aperture optical telescope – both periodic and random piston and segment tip/tilt errors, and (3) temporal bandwidth error. Various other effects such as segment tip/tilt errors, beam-train vibration, tip/tilt mirror (TTM) and deformable mirror (DM) offload related errors will also contribute to the residual aberration.

The performance of an AO system is primarily defined by the magnitude of the uncorrected aberrations, including residual aberrations, present in the system. Typically, the residual aberrations are either not seen by the AO system or seen but misinterpreted due to calibration errors or interference/diffraction fringes caused by effects such as segment piston errors, biasing the wavefront sensor (WFS) measurements.

We present sensing random piston errors through a phase retrieval approach using the science imaging instrument, NIRC2. Also, we explore the using the pyramid wavefront sensor (PyWFS) on Keck II as a piston error sensor and present the initial results.

The presence of a staircase mode on the Keck telescope primary mirror segments was previously found and compensated, resulting in a ~ 23% increase in the Strehl ratio in the Bracket-gamma filter (2.16 μm) for low elevation AO observations [4]. Subsequently, we incorporated this effect in the primary mirror active control system for routine telescope operation. We generalized this technique by projecting the segment pistons to a Zernike basis and present all possible periodic piston errors in the Keck segmented telescopes in this paper.

This article aims to infer the presence of low-order aberration in the optical system and the segment phasing errors of the telescope's primary mirror and take the necessary corrective measures. The broad objective of the work is to understand the residual wavefront errors and take appropriate actions to mitigate them where possible. The ultimate goal is to push the large aperture ground-based telescopes to their limits and make them as competitive as the space telescope in terms of PSF stability to enable breakthrough science.

The organization of the paper is as follows: the current state of the Keck AO systems in terms of the wavefront error budget is presented in Section 2; the concept of residual wavefront controller (rWFC) is introduced in Section 3; the static and semi-static aberrations are presented in Section 4; the dynamic aberrations are presented in Section 5; a discussion is provided in Section 6; and the summary, including a brief discussion of the results in the context of possible future AO upgrades and the next steps, is presented in Section 7.

2. THE KECK AO ERROR BUDGET

A parametric model based excel spreadsheet and a physical optics simulation model are used to understand the Keck AO system error budget and to make performance predictions. The parametric model treats the error terms as statistically independent, while the physical optics better grasps the correlation between error terms but contains fewer terms. An atmospheric model is used based on long-term seeing measurements.

The error budget tools have been anchored against error term specific tests and on-sky measurements. Table 1 shows the excellent resultant correlation between the excel spreadsheet computed Strehl ratio and full-width-at-half-maximum (FWHM) and the on-sky measured values for long-term NGS and LGS AO checkout data using a ~10^{th} magnitude NGS, and LGS AO Galactic Center science observations using a 20″ off-axis NGS [8, 9]. To achieve this correlation an additional 130 nm rms of high order wavefront error had to be added to the error budget for all cases and an additional 7 mas rms of tip-tilt for the LGS AO cases.

Table 1: Error budget tool predictions versus on-sky measured performance. The excellent agreement required adding 130 nm rms of high order error to all cases and 7 mas rms of tip-tilt to the LGS cases (nightly and Galactic Center).

Case	λ	Strehl Ratio		FWHM (mas)	
		Meas	Pred	Meas	Pred
Nightly NGS	K	0.53	0.53	50	50
Nightly LGS	K	0.44	0.44	53	53
Galactic Center	K	0.30	0.30	60	60
	H	0.16	0.17	64	64

The excel spreadsheet contains ~ 30 error terms. The terms that contribute > 30 nm rms of wavefront error to the LGS AO error budget are shown in Table 2.

Table 2: Error terms contributing ≥ 30 nm rms to the LGS AO case.

Science High-order Errors (LGS Mode)	Wavefront Error (rms)		Parameter		Science Band H	Science Band K
Atmospheric Fitting Error	121	nm	20	Subaps		
Bandwidth Error	133	nm	24	Hz (-3db)		
High-order Measurement Error	32	nm	20	W		
High-Order Aliasing Error	40	nm	0.3	Fitting reduction factor		
LGS Focal Anisoplanatism Error	153	nm	1	sci beacon(s)		
Uncorrectable Static Telescope Aberrations	66	nm	20	Acts Across Pupil		
Uncorrectable Dynamic Telescope Aberrations	74	nm		Dekens Ph.D		
Dynamic WFS Zero-point Calibration Error	50	nm		Allocation		
Residual Na Layer Focus Change	41	nm	30	m/s Na layer vel		
DM Finite Stroke Errors	31	nm	4.0	um P-P stroke		
Uncorrectable AO System Aberrations	30	nm		Allocation		
Uncorrectable Instrument Aberrations	60	nm		NIRC2		
HO Wavefront Error Margin	130	nm		Allocation		
Total High Order Wavefront Error	**312**	**nm**	**Strehl Ratio**		0.32	0.50
Science Tip/Tilt Errors	**Angular Error (rms)**		**Equivalent WFE (rms)**		**Parameter**	
Residual Telescope Wind Shake Jitter (one-axis)	2.6	mas	44	nm	29	Hz input disturbance
TT Error Margin	7.0	mas	116	nm		Allocation
Total Tip/Tilt Error (one-axis)	**7.7**	**mas**	**119**	**nm**	**Strehl Ratio**	0.87 / 0.89
Total Effective Wavefront Error			**315**	**nm**	**Strehl Ratio**	0.28 / 0.44
					FWHM (mas)	48.3 / 52.5

The largest error terms in Table 2 have been driving many of the current and planned upgrades to the Keck AO systems:

- Atmospheric fitting error and uncorrectable static telescope aberrations will be reduced by the proposed HAKA (High order All sky Keck Adaptive optics) project to replace the current 349-actuator Keck II deformable mirror with 7 mm actuator spacing with an ALPAO deformable mirror with 2.5 mm actuator spacing (Section 6.2.)
- Bandwidth error will be reduced by the NSF MRI and MSIP funded projects to replace the Keck II and Keck I real-time controllers, and wavefront sensor cameras, with faster systems. [10]
- Focal anisoplanatism error will be reduced by the NSF MSIP funded KAPA (Keck All sky Precision Adaptive optics) project to implement a four LGS asterism on Keck II. [11]
- The tip-tilt error margin has been demonstrated to be reduced on Keck I using a near-infrared tip-tilt sensor. [12, 13]
- Multiple of the remaining error terms, especially the 130 nm rms of high order (HO) wavefront error, are the subject of this paper and the proposed rWFC.

2.1 Point-spread function reconstruction (PSF-R) experience

The point spread function reconstruction (PSF-R) research at WMKO has shown measurable static residual wavefront aberrations in the Keck II NGS AO observations through on-sky phase diversity measurements [14,15]. The reconstructed

PSFs reproduce the low-order features in the observed PSFs very well after incorporating the estimated on-sky static phase map with an RMS wavefront error of ~ 100 nm (figure 13 of [16].) However, even after accounting for these presumably static wavefront errors, the Strehl ratio of the on-sky PSFs, taken with the Fe II filter (λ_{eff}=1.6455 μm) was found to be ~12% smaller than the reconstructed PSFs [16], corresponding to another ~ 90 nm rms of residual wavefront aberrations of somewhat unknown origin. The total Keck II NGS AO inferred residual wavefront error is therefore ~ 135 nm when the system is well-calibrated and optimized for the PSF reconstruction experiment, consistent with the error budget tool estimation of ~ 130. The residual aberration in the system during routine science observations could be more than this value, especially if an incorrect seeing value is used while acquiring the target or the telescope segments are not well-phased. Minimizing or eliminating the inferred residual wavefront errors would enable PSF-R, perhaps from high-fidelity simulation without the need for AO telemetry, besides improving the AO performance for science.

3. RESIDUAL WAVEFRONT CONTROLLER CONCEPT

We propose a new subsystem, a residual wavefront controller (rWFC), to monitor the performance of the AO and the environment and make necessary changes to minimize the wavefront residuals. This is a distributed subsystem consisting of hardware and software modules at the telescope, AO system and the science instruments. A schematic diagram of the proposed subsystem is shown in Figure 1.

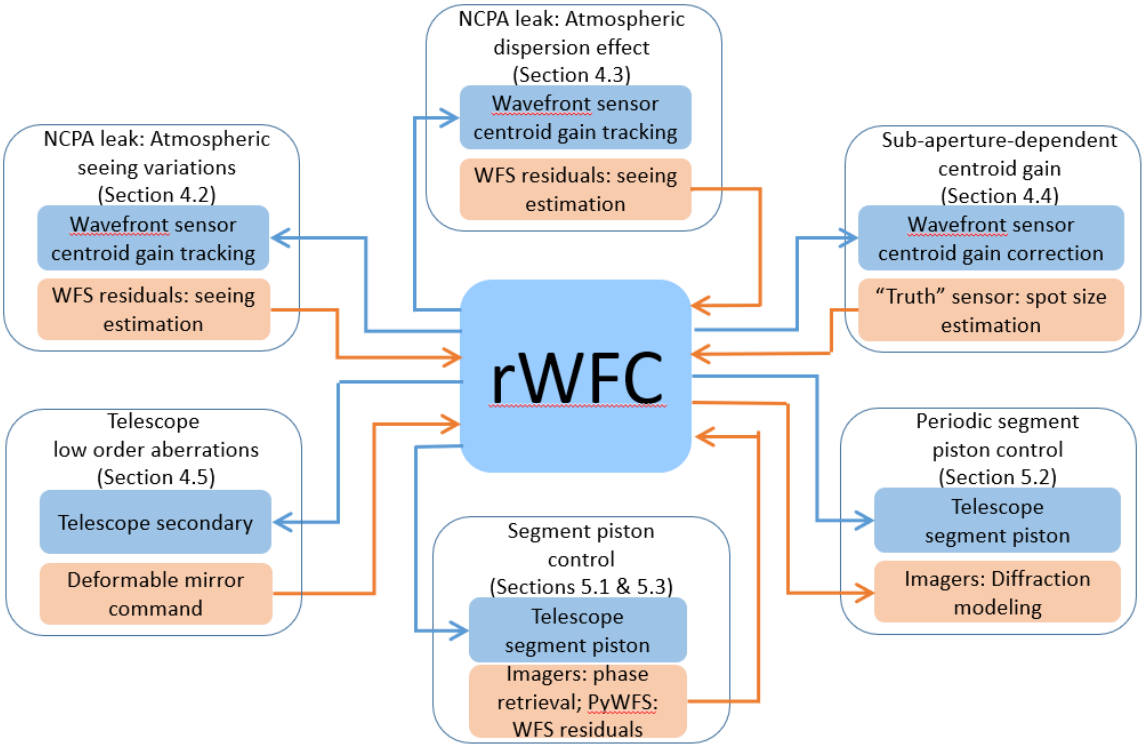

Figure 1: A schematic diagram of the components of the residual wavefront controller.

The rWFC provides multiple feed-back loops outside the traditional fast AO loops. It uses time-averaged WFS residuals and DM commands, and several other sensors and actuators, to optimize the performance of the AO system. The initial work on some components of the proposed subsystem is presented in Sections 4 and 5.

The main components are: (1) non-common path aberration (NCPA) leakage due to seeing changes (Section 4.2), (2) NCPA leakage due to atmospheric dispersion effect (Section 4.3), (3) sub-aperture-dependent centroid gain (Section 4.4), (4) telescope low order static aberrations (Section 4.5), (5) random piston errors (Section 5.1), and (6) periodic segment piston errors (Section 5.2). We have listed a handful of additional items in Section 6.1 that will be investigated for possible inclusion in the rWFC.

In addition to adding more control loops, rWFC would provide additional information on a few existing offload loops and auto analyse the data to improve the telescope performance. The objective is to improve the performance by optimizing the parameters for compensation models such as telescope pointing and telescope focus and thereby reducing the need for frequent offloading (Section 6.1.2.)

4. STATIC AND SEMI-STATIC ABERRATIONS

In this section, we present the optical effects and calibration biases that tend to be predominantly static or semi-static. This classification includes effects such as the NCPA leakage, the low order aberrations from the telescope, calibration biases, and sub-aperture-dependent spot size and spot elongation.

The static or semi-static effects may be sensed and characterized, and an appropriate model can be applied to the tracking points of the telescope control systems, as in the case of the staircase mode. The dynamic components of the effects, on the contrary, would require real-time measurement and correction capability. A dynamic effect accounted for as static could do more harm than good. For instance, the primary mirror segment petal mode proposed earlier [4] appears not static enough to apply routine correction to the primary mirror active control system.

4.1 Non-common path aberration (NCPA) leakage

The Shack-Hartmann (SH) wavefront sensor (WFS) measures the centroid offsets. These measurements are converted to wavefront slopes through a scale factor, centroid gain or optical gain. The error in the centroid gain is likely the major contributor to the static aberrations seen in the Keck AO systems, as quad-cells are used where the centroid gain depends on the spot size and spot elongation. This wouldn't be an issue from a static aberration standpoint if the WFS was operated at null. Unfortunately, the AO systems are operated significantly off null due to non-common path aberrations. Hence, effectively a factor of the off-null reference slopes leaks into the system when the centroid gain used in the system is not accurate.

The NCPA is estimated in the daytime using the white light source. A part of the NCPA will leak into the system if the centroid gains are incorrect. The resultant $NCPA_{leak}$ could be estimated as follows, assuming the centroid gain used for daytime calibration is accurate.

$$NCPA_{leak}(t) = \left(\frac{\delta g_{sky}(t)}{g_{sky}(t)}\right) NCPA \quad (1)$$

Where $g_{sky}(t)$ is the instantaneous on-sky centroid gain estimated from the spot size for the given seeing condition and the source size and $\delta g_{sky}(t)$ is error in $g_{sky}(t)$ - the difference between the optimal centroid gain and the centroid gain in use. The effect of $NCPA_{leak}$ also negatively impacts the temporal bandwidth of the AO, which will be discussed under the dynamic aberration session (Section 6.1.1.1).

4.1.1 NCPA in the Keck AO systems

For the same on-sky target, the optical path to the science instrument and WFS are common through most of the AO system. Non-common path aberrations (NCPA) are introduced by (1) a tilted dichroic beamsplitter, in the converging beam transmitted to the science instrument, that reflects the visible light to the SH WFS; (2) a second tilted dichroic beamsplitter that can be inserted in front of the science instrument to send light to a near-infrared sensor; (3) the science instrument optics; (4) a tilted beamsplitter in the WFS path; and (5) the WFS optics. The static aberrations in the path to the science instrument detector are compensated with the DM for AO operations; resulting in all the NCPA contributions being seen on the WFS. The aberrations measured by the SH WFS for three science instrument configurations are shown in **Figure 2** (left.) Sample Keck I OSIRIS imager (OSIMG) exposures when the SH WFS is operated at null (top) and when the WFS operates off-null to have the best image quality on the science camera (bottom) is shown in **Figure 2** (right.)

Additional NCPA will be seen on the SH WFS as a result of (6) moving off-axis with the WFS and (7) moving to a different conjugate altitude when the SH WFS is using an LGS.

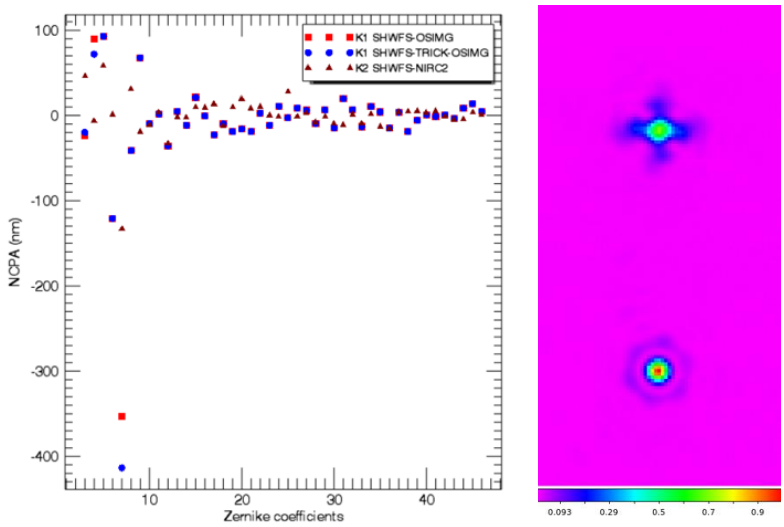

Figure 2: Left: Aberrations present on the Shack-Hartmann (SH) wavefront sensor (WFS) when the deformable mirror is optimized for three science instrument configurations: The Keck I OSIRIS imager (OSIMG), with and without the dichroic that feeds the near-infrared tip-tilt sensor (TRICK). The Keck II NIRC2 imager without the dichroic that feeds the PyWFS. Right: Keck I OSIRIS imager (OSIMG) exposure when the SH WFS is operated at null (top) and when the WFS operates off-null to have the best image quality on the science camera (bottom.)

4.1.2 Astigmatism correctors

The dominant NCPA seen in the SH WFS path is astigmatism introduced in transmission through the tilted dichroic beamsplitters (and compensated with the DM). A wedge in the second surface of the dichroic could be used to compensate for astigmatism; however, a second surface wedge is already being used in the science path dichroics to compensate for lateral chromatic aberrations instead. The existing wedge overcompensates for the astigmatism introduced by the tilted dichroic, such that a plate tilted in the orthogonal direction in the WFS arm would be needed to compensate for the astigmatism correction applied to the DM. Options to reduce the astigmatism NCPA include (1) introducing a wedged plate in the WFS neutral density filter slide or (2) acquiring a new science path dichroic with a cylindrical second surface.

Even with the astigmatism correctors, active NCPA leakage corrections will be needed as there are other astigmatism terms besides astigmatism in the Keck NCPA. The proposed rWFC would track the centroid gain variation to minimize/eliminate the NCAP leakage.

4.2 NCPA leakage due to seeing change

While acquiring the targets. the AO acquisition tool (AOacq) sets the centroid gain based on the seeing value provided by the operator and the centroid gain values used during the daytime AO calibration using a white light single-mode fiber source. An incorrect seeing or centroid gain setting during the AO calibration would result in an incorrect on-sky centroid gain and hence incorrect reference slopes. An automated seeing-based approach was implemented [16] but not released to routine operation as the approach requires a variable fudge factor, possibly due to the varying phasing status of the primary mirror. The tool will be compared with other approaches, such as the tip-tilt (or a higher order) modulation at a rate larger than the control bandwidth of the AO system to calibrate the centroid gain as part of the rWFC implementation.

Figure 3 (left) shows the NCPA leak as a function of percentage error in the on-sky centroid gain parameter, and Figure 3 (right) shows the NCPA leak as a function of seeing, assuming that the user left the AOacq seeing setting at the default value of 0.75″, which is typically the case during the science operation.

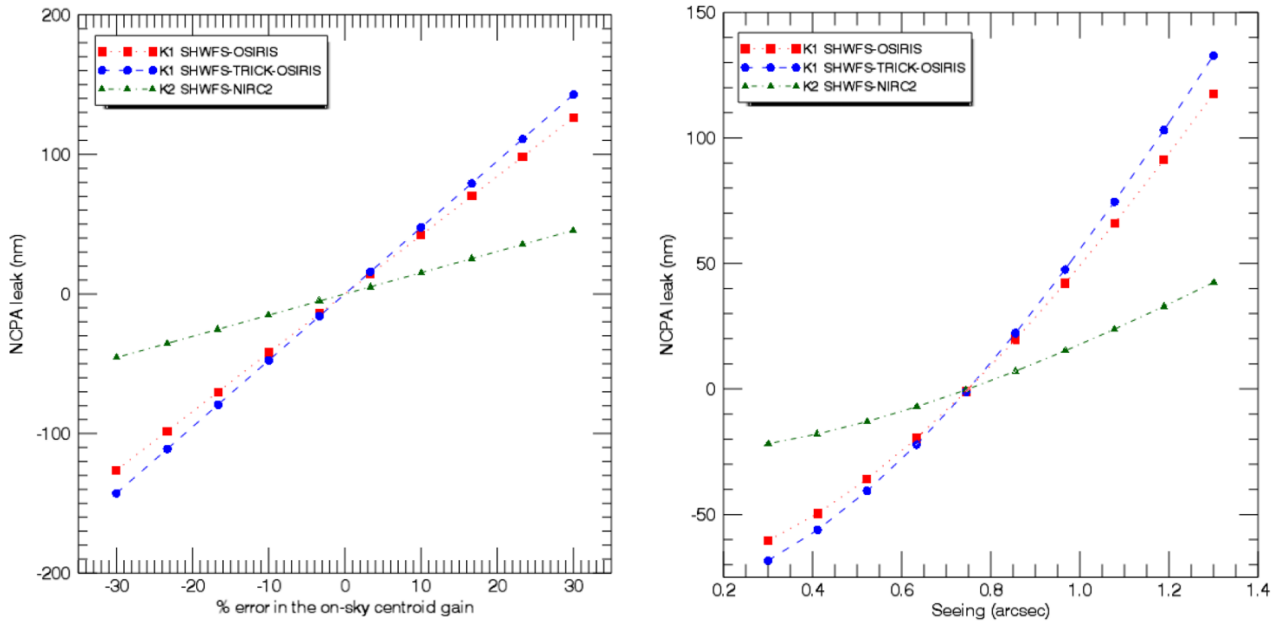

Figure 3: Left: NCPA leakage with % error in the centroid gain. Right: NCPA leakage with seeing, assuming the user left the AOacq seeing value at the default value of 0.75″.

4.3 Centroid gain correction for atmospheric dispersion effect

Atmospheric dispersion plays a significant role in biasing the WFS measurements, especially for low elevation NGS AO observations using the SH WFS that operates at visible wavelengths. The optical bandwidth of the WFS is defined by the spectral response of the CCD camera used in the visible wavelengths. Figure 4 (left) shows the atmospheric dispersion computed for the SH WFS CCD39 detector with zenith distance. The estimated spot broadening at a zenith distance of 60° along the elevation axis is ~2″. Figure 4 (right) shows the expected NCPA leak due to the spot elongation introduced by the atmospheric dispersion, assuming a seeing of 0.5″. The estimated NCPA leak for K1 SHWFS-OSIRIS, K1 SHWFS-TRICK-OSIRIS, and K2 SHWFS-NIRC2 configurations at 45° elevation are 104, 117, and 38 nm, respectively, at 0.5″ seeing.

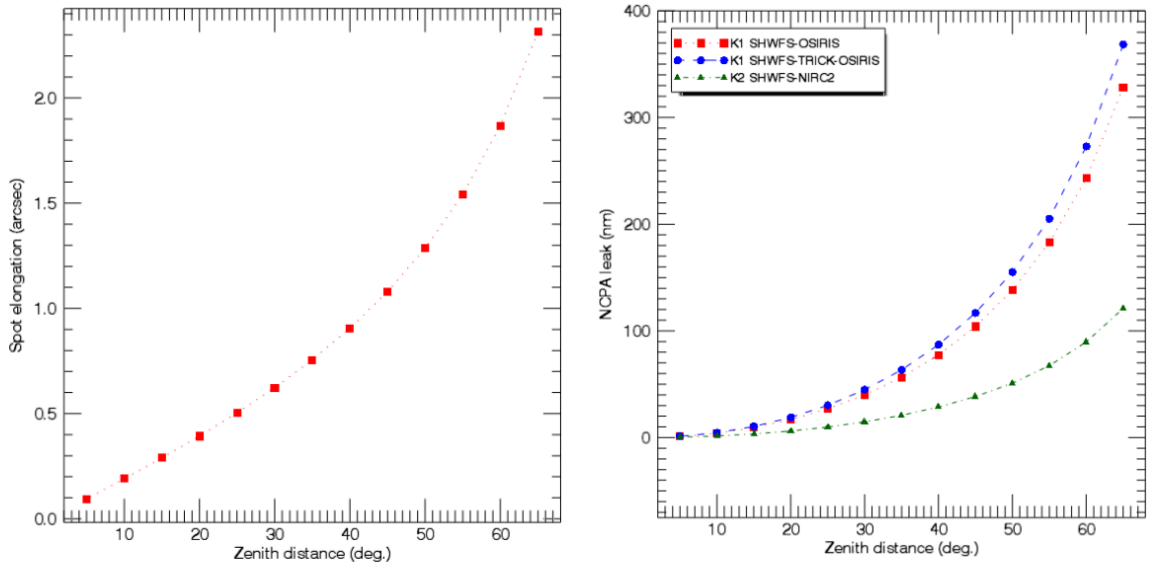

Figure 4: Left: The contribution of atmospheric dispersion to spot size along the elevation axis. Right: The corresponding NCPA leak for three instrument configurations.

The effect could be addressed by scaling the centroid gain. However, the error in the spot size estimation would limit the degree of dispersion compensation thorough centroid gain scaling. The ultimate solution is to introduce a dispersion compensation system in the AO system (Section 6.1.4.)

The spot elongation due to atmospheric dispersion will also reduce the control loop bandwidth (Section 6.1.1.1), resulting in additional performance deterioration.

4.4 Sub-aperture-dependent centroid gain

In addition to the two effects mentioned above, the spot sizes of individual sub-apertures could be different for other reasons, such as aberrations from individual primary mirror segments. Measuring the spot size and spot elongation of individual sub-apertures of the WFS, perhaps infrequently, would enable accounting for these effects.

The sub-aperture-dependent centroid gain was previously tested in daytime calibrations through a scanning approach [16]. Subsequently a dithering approach for on-sky calibration was attempted but was found to be unstable. More recently, we used the "truth" sensor to estimate the sub-aperture dependent spot size and hence the sub-aperture-dependent centroid gains on the sky. A set of 10 exposures were taken in non-binning mode to improve the accuracy of the spot size and spot elongation measurements. The sub-aperture images show measurable elongation with the direction of elongation aligned to the X-axis – the elevation axis of the telescope for these measurements. The atmospheric seeing during these observations was 0.6″.

The estimated X and Y spot sizes for each sub-aperture of the LBWFS "truth" sensor is shown in Figure 5 (left). The sub-apertures are sorted with spot size difference between the X and Y axes to highlight the spot size differences. For clarity, only the sub-apertures that have a size difference above the 1 sigma measurement noise (209 out of 236; i.e., 89% of the illuminated sub-apertures) are shown. The median X and Y spot sizes are 0.73 ± 0.07″ and 0.56 ± 0.08″, respectively. The measured spot size along the azimuthal axis of 0.56″ at an effective wavelength of 640 nm is consistent with the estimated seeing 0.6″ at 500 nm. The measured spot elongation of ~ 0.47 ± 0.11″ is somewhat smaller than the expected value of 0.62" due to atmospheric dispersion effect (Figure 4 (left).)

Figure 5 (right) shows the expected NCPA leak due to the sub-aperture-dependent spot size and spot elongation; i.e., with respect to the difference between median size along the X- and Y-axes, meaning that the effect of overall spot elongation is excluded in this estimation to avoid double-counting this effect, since the dispersion compensation (Section 4.3) should account for this to first order. The model is computed for different seeing conditions. As expected, the effect will be dominant for excellent seeing conditions and has negligible contributions for good to bad seeing conditions. There may be other effects such as sagging of the primary mirror due to gravity that could potentially introduce spot elongation. These effects will be investigated, and appropriate corrections applied through the rWFC.

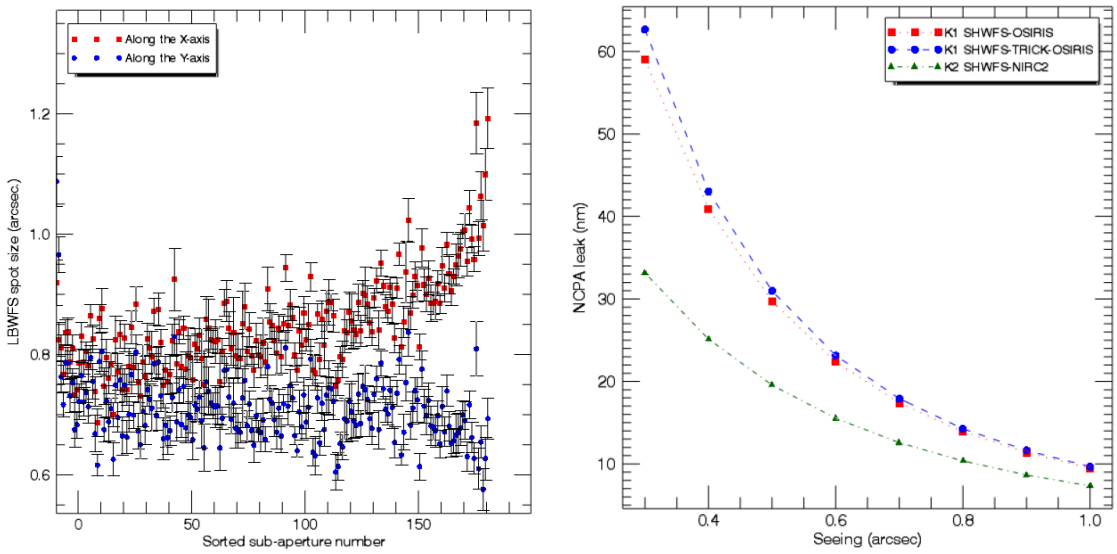

Figure 5: Left: Sub-aperture spot size from the "truth" WFS along the X and Y axes. Right: The corresponding NCPA leak versus seeing for three instrument configurations.

4.5 Telescope static aberrations

The telescope optics are not part of the optical path used during the daytime AO calibration. Since the telescope optics are in the common path to the WFS and the science instruments, excluding them for AO calibrations has little direct impact to AO calibration and the AO system largely corrects for the telescope aberrations. However, the presence of a significant low order aberration in the system would take the dynamical range of the DM, limiting the range available to account for atmospheric turbulence and local disturbances. The presence of a large static aberration would cause reconstruction errors and actuator coupling issues, resulting in some high spatial frequency static aberrations in the system in the WFS and the science paths. In addition, the presence of significant static aberration would bias the focus error estimated by the WFC from the DM shape, resulting in incorrect focus offload to the telescope secondary and hence slightly defocused images on the science instruments.

The telescope pupil rotates with respect to the AO system during science observations to keep the sky orientation fixed on the science instrument. As a result, the AO performance could vary as the mapping of the low order aberrations from the telescope to the sub-apertures and the DM actuators change - especially for the central and the outer regions of the pupil as the slaved actuators corresponding to the non-illuminated actuators change with pupil rotation. The ability to measure but not correct could potentially drive the corresponding DM actuators to saturation, further adding static residuals.

The time-averaged DM commands contain the information of the low order static aberrations sensed and corrected by the AO. A sample on-sky residual static Keck I and Keck II AO DM shape, after subtracting the contributions from the WFS reference slopes, is shown in Figure 6 (left.) Also shown in the figure are decomposed Zernike phase maps – Z5 through Z44 (middle) and only the coma terms (right.) The dominant error terms are coma (2448 nm on Keck I and 561 nm on Keck II) and astigmatism (967 nm on Keck I and 482 nm on Keck II). The RMS wavefront error of the combined contribution from coma and astigmatism is 2632 nm on Keck I and 740 nm on Keck II.

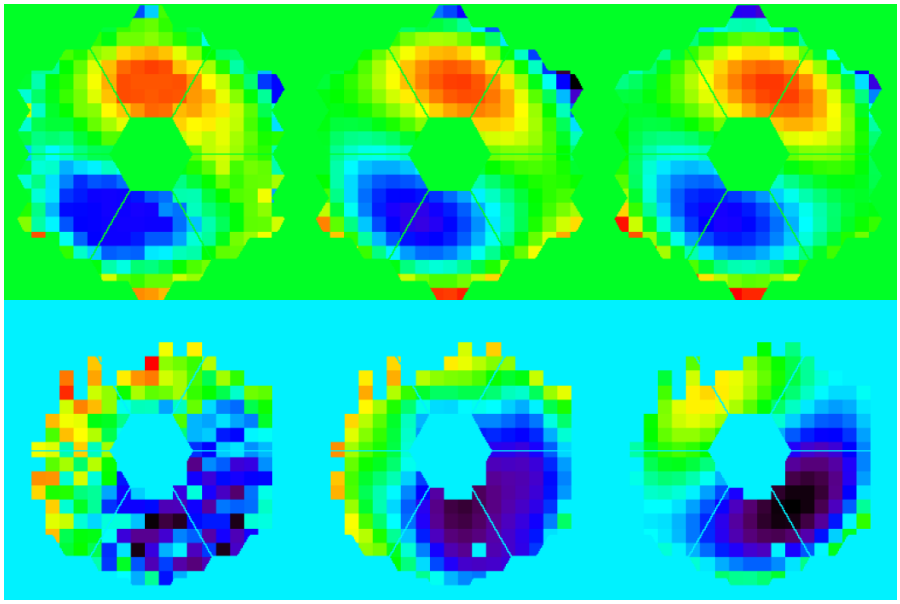

Figure 6: Left: A sample on-sky residual static DM shape on K1AO (top row) and K2AO (bottom row), after subtracting the contributions from non-common path aberration. Middle: Corresponding Zernike decomposition (Z5 through Z44). Right: Coma only.

The Zernike coefficients from Z5 (45°-astigmatism) through Z44 coefficients are shown in Figure 7.

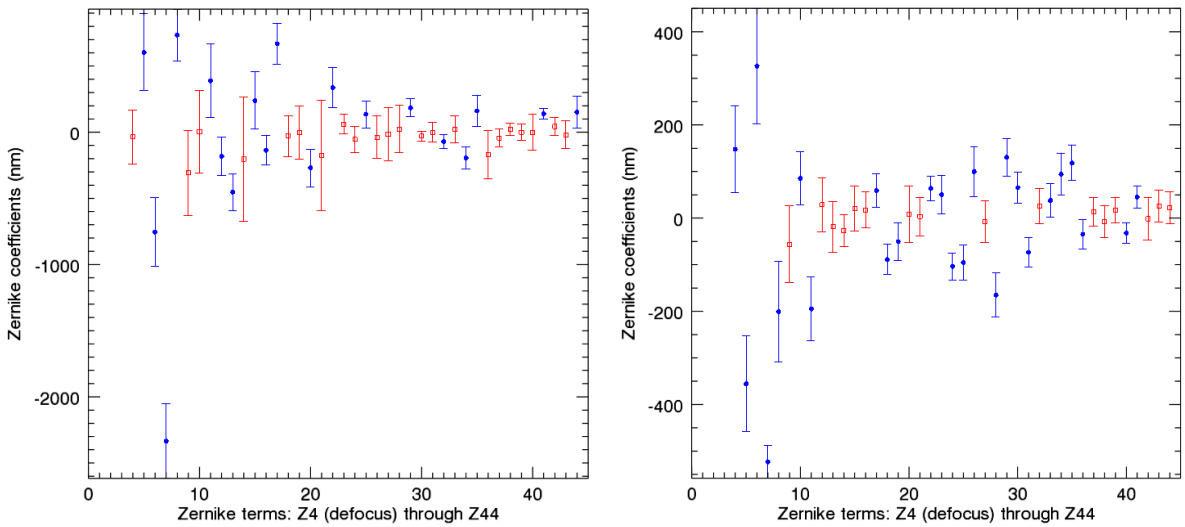

Figure 7: The Zernike coefficients from Z5 (45° Astigmatism) through Z44 on K1 AO for Keck I (left) and II (right).

4.5.1 The source of the low order aberration

The telescope optics are primarily responsible for the aberrations presented in this section as the NCPA contributions are removed from the estimated aberrations.

The entrance of the AO system is equipped with rotator optics (a K-mirror configuration) to compensate for the pupil or the field rotation on the science instrument while tracking the targets. If the aberrations were to come from the telescope, then they would rotate with telescope pupil orientation. On the other hand, if the aberrations were to come from the AO system, the features seen in the reconstructed phase maps would be fixed. Figure 8 shows the reconstructed phase map with the telescope pupil orientation on Keck I. As can be seen, the low order features in the phase map are fixed to the telescope pupil, confirming that the observed low order aberrations indeed come from the telescope.

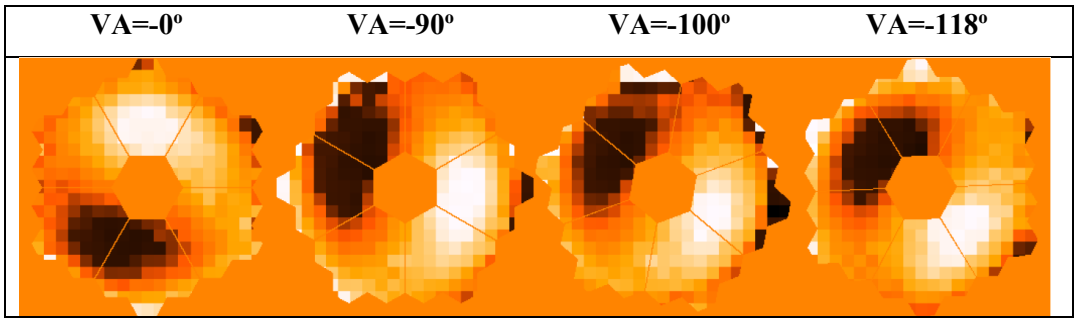

Figure 8: Phase map with telescope pupil orientation on Keck I.

A ray-tracing analysis of the on-axis optical performance of the Keck telescope and the AO optical system shows that the expected theoretical wavefront error in the optical system, in the absence of any additional static aberration, is 82 nm RMS and the off-axis performance at 60″ is 109 nm RMS. The dominant on-axis error term is astigmatism: 79 nm RMS. These relatively low amplitude aberrations are corrected by the AO system with very little to no impact on the AO science instruments.

Now, we consider a scenario where the telescope secondary mirror is decentered and/or tilted. The decentering error could be compensated by appropriate tilt error, and hence varying amplitude of tilt error is introduced in the ray-tracing model of the optical system to mimic both effects. The resultant on-axis wavefront error for the coma and astigmatism terms with the tilt angle is shown in Figure 9. A decentered and/or tilted telescope secondary mirror with an equivalent error of ~350″ on K1 and 83″ on K2 telescopes would explain the coma seen by AO.

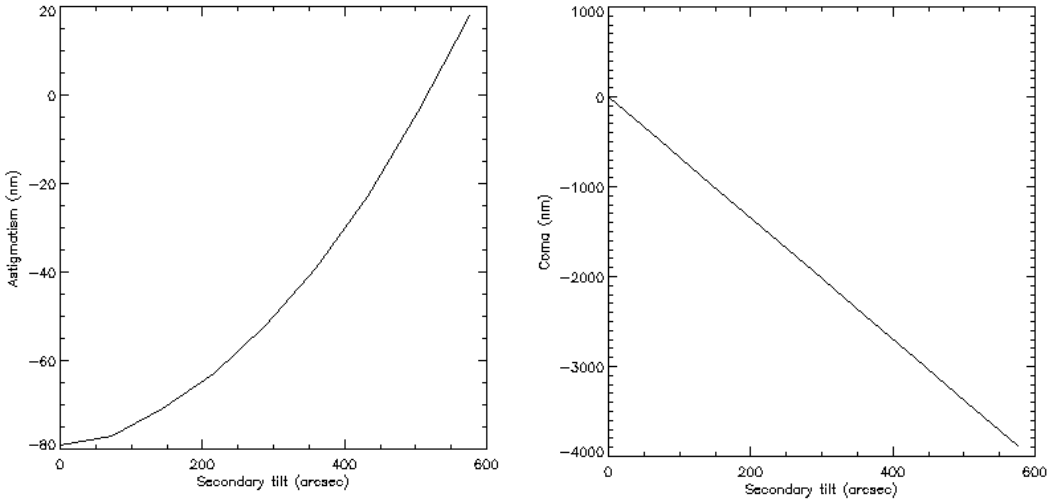

Figure 9: The estimated RMS error with secondary tilt for astigmatism (left) and coma (right).

The proposed rWFC would estimate the low order aberration terms, including the coma, and will be offloaded to the telescope's secondary tilt. The infrastructure to command the telescope secondary exists but the coordinate transformation needs to be defined and tested. The AO reconstructor could be modified to include an estimation of coma contribution seen by the WFS, or a standalone high-level software tool could estimate this from the DM command telemetry and apply corrections to the telescope secondary. In addition, the information will be made available for telescope operation so that the secondary tilt, if any, will be corrected for the other instruments as well.

5. DYNAMIC ABERRATIONS

Almost all residual wavefront effects, including those presented in Section 4, have at least some dynamic components. Dynamic aberrations are challenging as they require real-time sensing and compensation, especially the sensing techniques that require dedicated telescope time. If the variability timescale is less than an hour or difficult to characterize in term of measurable parameters, it may impractical although not impossible to account for these effects. On the other hand, most of the dynamical effects are likely to have some static and semi-static component and those are the primary target for rWFC. We briefly discuss four cases in this category. They are residual segment piston error, temporal bandwidth drift, vibration, and tip/tilt, DM and differential atmospheric refraction (DAR) offload-induced errors.

5.1 Residual segment piston errors

The Keck telescope segments are typically phased every two months. The segment phasing drifts between phasing operations. The segment phasing may initially drift rapidly (dynamic) and then stay reasonably constant (static or semi-static), but this is yet to be confirmed.

Typically, the SH WFS does not see the piston errors, but the uncorrected residual piston errors affect the science images. The step-function introduced by the segment piston would introduce diffraction effects at the segment edges that will be misinterpreted as local slopes by the affected sub-apertures of the WFS, resulting in low-order aberrations. This section addresses the residual piston error uncorrected by the AO system. The uncorrected residual segment tilt errors are briefly discussed in the following section (Section 6.1.1.2.)

Science camera images taken with some diversity under stable atmospheric conditions with adequate signal-to-noise ratio could be used to estimate the segment piston errors [4]. Using a phase retrieval technique, we successfully demonstrated residual segment-piston-phasing using the NIRC2 imager on Keck II. The approach uses a modified Gerchberg-Saxon algorithm on defocused images. **Figure 10** shows a sample PSF before and after the residual piston correction using this algorithm. The PSF looks more symmetric after the piston correction. The Strehl ratio increased from 56% to 61% (a 7% increase) when residual segment piston phasing was enabled. The corresponding decrease in the RMS wavefront errors is 92 nm. We anticipate that the piston phasing improvements would have significant gains for high contrast imaging if the piston errors were predominantly static. It is unclear what fraction of these errors is static versus semi-static and dynamic. Once the nature and stability of these errors are understood, we will be able to feed-forward these biases to the primary

mirror active control system the same way we implemented the staircase mode compensation. More details on the technique are presented in a paper presented at the Ground-based and Airborne Telescopes IX conference at this SPIE meeting [17].

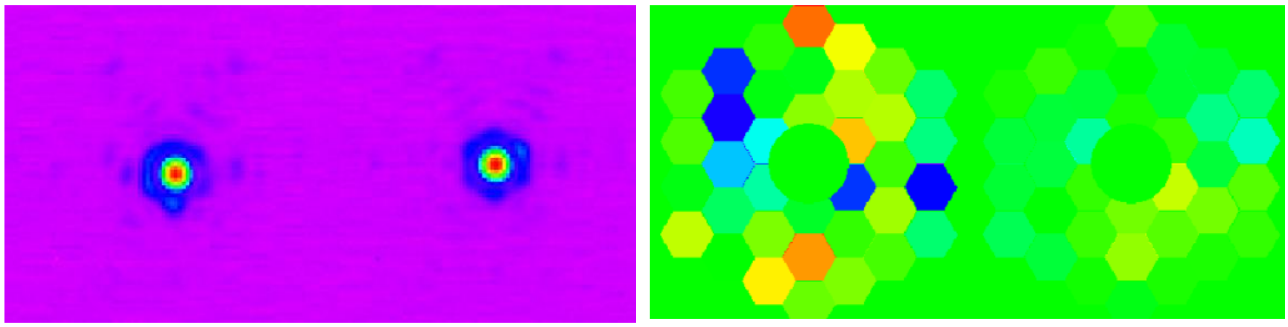

Figure 10: Left: Sample NIRC2 imager PSFs before (left) and after (right) segment phasing [17]. Right: The corresponding segment piston maps after the first and fourth phase retrieval iteration.

5.2 Periodic segment piston errors

Earlier, the presence of a primary mirror segment staircase mode was found on the Keck telescopes through an AO simulation-based approach, and appropriate corrections were applied to demonstrate the cancellation of two bright speckles present in the NIRC2 and OSIRIS science images. A ~ 23% increase in the Strehl ratio was demonstrated for low elevation AO observations of bright targets using the NIRC2 science camera in the Bracket-gamma filter (2.16 μm) after applying appropriate compensation for segment piston errors estimated [4]. We subsequently incorporated the staircase mode into the Keck telescope control system to account for this effect. The possible presence of petal mode was also proposed.

We generalize this technique by projecting the segment piston errors to the Zernike basis, meaning the center of the pistoned segments follows the Zernike functions. For instance, the tip/tilt term in the Zernike basis will represent the staircase case mode, and the trefoil term will closely represent the petal mode. The simulated piston maps corresponding to the first 20 Zernike modes starting from tip/tilt (i.e., Z2 through Z21) are shown in Figure 11.

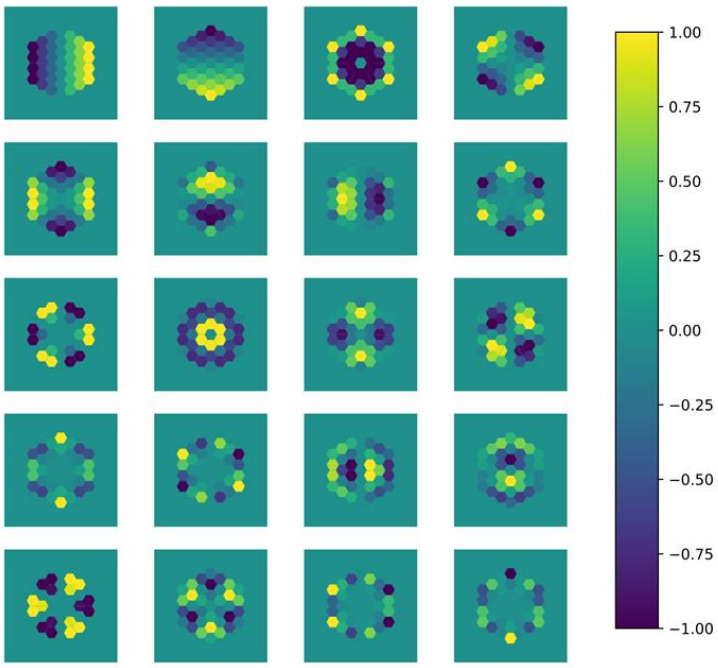

Figure 11: Piston map corresponding to the first 20 Zernike modes excluding the piston (i.e., Z2 through Z21.) Note we normalize each mode for visualization purposes.

The AO simulations were carried out using the HCIpy python package [18], and we assumed an RMS wavefront error of approximately 170 nm for each mode on the segmented primary. The Keck II AO system simulation with the same configuration as in [19] was used for this work. The turbulence was assumed to be von Karman with an r0 value of 15 cm and an outer scale of 50 m. The wind speed was chosen to be 10 m/s. Using the pyramid wavefront sensor operating in H-band at 1 kHz on a 5th magnitude star to control the 349-actuator DM, the corrected science light is sent through to the K-band vortex coronagraph to mimic the high-contrast observing configuration with the NIRC2 imager on the Keck II telescope. The typical Strehl ratio delivered to the coronagraph in K-band is greater than 60%. The resultant coronagraphic point spread functions (PSFs) are presented in Figure 12 for the first 20 Zernike modes (starting from Z2) corresponding to Figure 11.

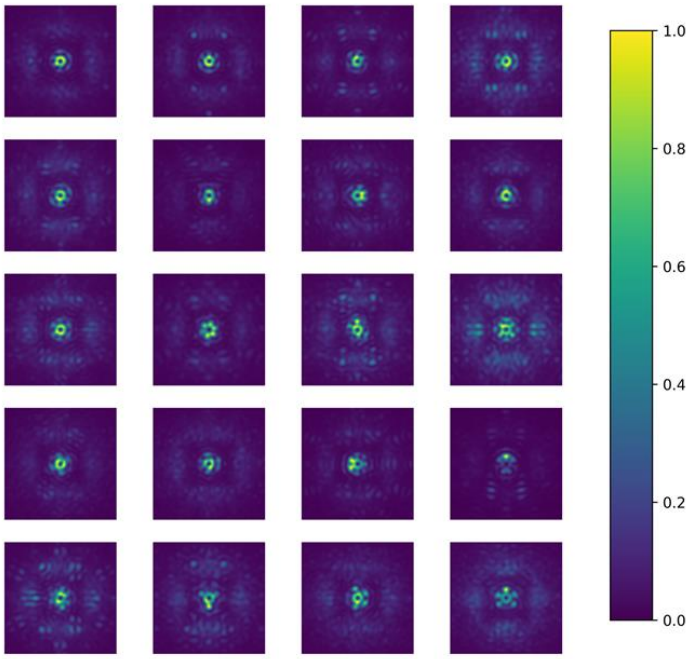

Figure 12: The simulated NIRC2 PSFs for potential periodic segment piston errors in the Keck telescopes.

The next step is to search the archived NIRC2 images of bright science targets, especially the high-contrast imaging observations, for the possible presence of any of these periodic modes. We will also explore the Phasing Camera System (PCS) data before and after the telescope phasing for possible presence of these modes. The periodic modes will be apparent even for a small amplitude piston as all 36 segments contribute to the piston error signals [4]. We will feed forward these errors, if any, to the primary mirror active control system the same way we addressed the staircase mode earlier.

5.3 Pyramid wavefront sensor for piston measurements

We are exploring the possibility of using the Keck II near-infrared pyramid wavefront sensor for measuring residual segment piston errors. The first set of measurements is presented in this section, along with a preliminary analysis through AO simulations.

The observations involve (1) taking reference WFS slopes and DM commands measurements and (2) taking measurements after pistoning three segments in a letter L pattern to verify segment mapping. We applied a sequence of piston amplitudes, 50, 100, 200, and 400 nm, to the three segments. The resultant differential slopes and DM commands with respect to the reference are presented in Figure 13.

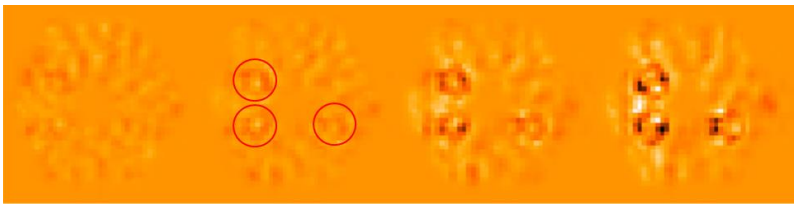

Figure 13: The measured differential slope map with piston amplitude. Differential slopes in the X-axis for piston amplitudes of 50, 100, 200 & 400 nm (left to right.) The three pistoned segments are marked with red circles for one of the four cases corresponding to 100 nm segment piston.

The simulated slopes for the Keck II AO configuration using the HCIpy python package [18] are shown in Figure 14. The AO model used in the simulation is far from the real system but shows the signature of segment piston errors in all but the 400 nm piston cases.

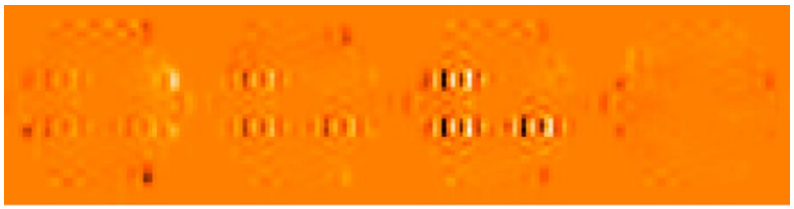

Figure 14: Simulated X-slopes for Keck II AO with piston amplitudes of 50, 100, 200 & 400 nm (left to right.)

The DM commands do not show the signature of segment piston errors. We anticipate seeing the effect when we upgrade the Keck II DM with a higher-order DM as part of the HAKA project (Section 6.2).

While our primary interest is to measure segment piston error, if any, during routine AO science observations, we will also be exploring the possibility of phasing the segments after the segment exchange using the PyWFS, especially once the high order WFS for the HAKA project is in place. We will also be exploring the possibility of sensing residual low-order aberrations using the PyWFS. As a precursor, we plan to test this approach with the PyWFS MEMS.

Simultaneous use of the SHWFS and PyWFS is another approach we are looking into to take advantage of obtaining complementary information to sense residual wavefront aberrations. In this configuration, we will be using the SHWFS in closed loop while the reconstruction process of the PyWFS will be optimized to sense the segment piston errors. An alternate approach to measuring segment piston errors is using the ZWFS [25] on Keck II, implemented as a part of the KPIC project. [24]

6. DISCUSSION

We attempt to answer the question we raised in the introduction: whether the first generation segmented mirror technology and the adaptive optics are ready to (1) take on the challenges of high contrast imaging to characterize habitable zone exoplanets, (2) fully benefit from recent extreme AO developments, and (3) enable visible AO science?

As of today, the answer is probably a no. However, we expect that the proposed rWFC in conjunction with the reduced fitting and aliasing errors through HAKA (Section 6.2) on Keck II and reduced focal anisoplanatism error through KAPA on Keck II [12] would enable us to answer yes to these questions, especially if a significant part of the residual aberrations are found to be static or semi-static. A few additional error terms to be added to the rWFC are briefly mentioned in Section 6.1, and the HAKA project, upgrading the Keck II DM (349 actuators) with a high-order one (over 3000 actuators), is presented in Section 6.2.

6.1 Residual Wavefront Controller additions

The complete rWFC includes (1) additional error terms (Section 6.1.1) besides the ones mentioned previously, (2) optimization of the offloads to the telescope (Section 6.1.2), (3) AO calibration improvements (Section 6.1.3), (4) hardware upgrades (Section 6.1.4), (5) trade-off studies and optical design for potential future upgrades (Section 6.1.5), and (6)

additional sensors and actuators from other development projects (6.1.6). In addition, the rWFC would include archival, logging and reporting options.

6.1.1 Additional error terms

6.1.1.1 Non-optimal temporal bandwidth

The effect of non-optimal centroid gain, mentioned in Sections 4.2 through 4.4, results in non-optimal temporal bandwidth besides static aberrations. While the static aberrations due to incorrect centroid gain could be avoided through optical means (Sections 4.1.2 & 6.1.4), the negative impact for temporal bandwidth cannot be avoided this way. A lower centroid gain than the optimal value would reduce the temporal bandwidth of the control loop. In comparison, a higher centroid gain would lead to instability in the control loop resulting in oscillations. The ongoing real-time controller upgrade [10] will provide a flexible infrastructure to implement a more stable centroid gain tracking for the Keck AO system.

6.1.1.2 Segment tip/tilt errors

The segment tilt/tilt positions also drift beside the segment piston. Segment tip/tilt is not a major concern since the AO system largely sees the segment tilt errors and compensates for them. However, to maximize the DM dynamical range for turbulence corrections and minimize the reconstruction errors, we should find a way to sense and compensate for the segment tip/tilt errors. The current actuator sampling of the DM per segment is not adequate to sense this error. We expect the HAKA upgrade (Section 6.2) to provide the necessary DM actuator sampling of the telescope segments to sense these errors. Meanwhile, we will be exploring other alternatives, such as tilting all segments by a known amount to make 36 spots on a fast camera and using the centroid error to measure the tip/tilt errors in AO open loop.

6.1.2 Wavefront controller offloads

The average position offset of the tip/tilt mirror, focus sensed by the DM, and the average differential atmospheric corrections are offloaded to the telescope pointing, the telescope secondary mirror, and the AO WFS pointing and centroid offsets, respectively.

Currently, the offload periods are seconds. The rWFC would track offload errors and provide input to improve telescope tracking and telescope secondary focus compensation model, reducing the offload period to minutes or longer with a goal of offloading errors only between science exposures. We propose implementing coma offloading to free up the DM range (4.5.1).

The focus sensed by the low bandwidth wavefront sensor (LBWFS) during LGS AO observations is offloaded to the telescope through the SH WFS focus stage (FCS) which ends up on the DM and then to the secondary. We propose a direct offloading of the focus errors sensed by the LBWFS to the telescope secondary to improve the performance of the LBWFS.

In the absence of an atmospheric dispersion compensator, the differential atmospheric refraction (DAR) correction is applied through software in the current system. Appropriate centroid offsets are applied to the SH WFS tip/tilt track point, and subsequently offloaded to the field steering mirrors (FSMs). If the centroid gain is incorrect, the DAR correction won't be accurate, and the target will drift on the science instrument during long exposures. rWFC would track the pointing drafts when a point source is available in the science frame and apply appropriate corrections to the centroid gain to improve the performance of the DAR compensation. In other words, an error in the DAR compensation could potentially be used as a sensor to optimize the centroid gain, as incorrect centroid gain would result in overestimating or underestimating the DAR compensation.

6.1.3 AO calibration improvements

The AO calibration is performed with a point source (10 μm diameter single-mode fiber) on the AO bench, and the AO calibration is validated on the science camera for closed-loop operation without turbulence. This would mean any error in the centroid gain will be unnoticed during the calibration check. The real-time controller (RTC) upgrade at WMKO [13] will allow us to introduce a DM-based turbulence simulator on both AO systems. We propose validating the AO calibration using the turbulence simulator and appropriate centroid gain once the RTC is upgraded.

The LGS AO calibration is performed with the source at infinity. This is because the fiber source cannot be placed at the position corresponding to 90 km on the AO bench due to the AO rotator located at the entrance of the AO system. Operating the WFS on-sky with the laser at a finite distance while the AO calibration is performed with a source at infinity introduces biases. This effect is not a significant issue from the static aberration standpoint as we use a "truth" sensor that drives the

reference WFS slopes to the optimal values. The effect could potentially be calibrated, and appropriate slope offsets added to the calibrated reference WFS slopes at infinity to minimize the need for the "truth" sensor. Moreover, the solution of applying offsets to the reference slope is not an ideal one as this won't address the temporal bandwidth drift due to the centroid gain drift. We propose applying corrections to the centroid gain through rWFC to address the static aberration and the temporal bandwidth issues simultaneously.

While the effect of subaperture-dependent spot size elongation due to the projection effect of the finite sodium layer thickness is accounted for in the current Keck AO systems, spot size or spot elongation drifts due to other optical and calibration effects are not taken into account. We propose addressing these effects using the "truth sensor", perhaps integrating longer to improve the SNR and in non-binning mode to improve the accuracy of the spot size measurements.

The AO calibration, typically performed in the afternoon, is not necessarily optimal as the AO bench temperature at night could be different and could vary throughout the night. The effect could be calibrated with AO bench temperature, and appropriate corrections applied to the calibration parameters during the observations.

The effects presented so far have focused on on-axis observations. However, even the on-axis observing sequence, let alone the off-axis observing, typically involves observing the targets at off-axis positions for sky subtraction. The NIRC2 imager exhibits field-dependent aberration [16, 20], and the effect could be minimized for narrow field AO observations by calibrating the AO system for a grid of NIRC2 field positions in the daytime and loading appropriate reference slopes and the WFS camera focus positions.

6.1.4 Hardware upgrades

We list below potential hardware upgrades as part of the rWFC development:

- Upgrade the dichroic beamsplitter substrates and the science camera window glass to reduce the aberrations in the science path.
- Implement an atmospheric dispersion corrector for the SH WFS operating in the visible wavelength for the NGS case.
- Locate the calibration source at the correct telescope focus position for the NGS and LGS calibrations. The NGS calibrations requires locating the fiber at infinity position, while the LGS calibrations requires this at distances as low as 85 km position.
- Perform some AO calibrations with a fiber core size equivalent to the median seeing at the summit to minimize the calibration errors.
- Perform certain AO calibrations with added turbulence in the AO system, especially while validating the daytime AO calibrations for night time observation.

6.1.5 Trade-off studies and optical design

We list below a list of trade-off studies and optical design to be performed as part of the rWFC development:

- Perform a quad-cell versus multi-pixel CCD sensor trade-off study. The use of multiple pixels would reduce the residual static wavefront errors due to WFS spot size change at the expense of reduced sensitivity. The recent detector technology development provides low noise and fast-readout optical and near-infrared sensors. We discuss below the trade-off between the quad-cell and the multi-pixel configuration.
- Perform a case study of the impact of vibration on the AO performance and design a vibration sensing system. The potential implementation includes (1) the use of parametric oscillators in the RTC through the proposed rWFC and (2) the addition of accelerometers on the telescope segments, secondary and tertiary mirrors, and the AO bench, if necessary.
- Investigate the dynamics of the tip/tilt and the deformable mirrors and upgrade them if necessary.
- Explore the possibility of introducing active optics in the WFS optical design to further mitigate the static aberration in the AO system. The use of active optics would enable accounting for relatively high order statics aberration, too, in the system. Perhaps one of the fold mirrors, such as the field steering mirrors may be replaced

with a low-order DM with sufficient dynamical range to account for other low order terms in the AO bench. Such implementation could enable applying focus offloads to this second DM instead of the telescope secondary.

- Explore the possibility of shifting the field/pupil rotation compensation task from the AO bench to the AO science instruments for future AO instruments.
- Design a compact and more stable visible and near-infrared WFS fore-optics that can be directly mounted to the WFS camera, and potentially cooled down to -30°C in the future for improved performance with the AO science instruments in the L- and M-bands. The design should have a target optical aberration of < 25 nm, including the switchyard dichroic. The aberration introduced by the dichroics should be accounted for in the dichroic substrate or the combination of dichroic substrate and the WFS camera window glass.

6.1.6 Additional sensors and actuators

Additional sensors or sensing techniques for the rWFC subsystem could be provided by the ongoing development activities at the Keck observatory, (1) speckle nulling [21], (2) Fast and furious focal-plane wavefront sensing [22], and (3) predictive control [23]. The Keck Planet Imager and Characterizer (KPIC) project [24] provides additional sensors (i.e. a Zernike wavefront sensor [25] and C-Red 2 focal and pupil plane sensor) and actuators (i.e. a MEMS DM [26]) as well as the near-infrared pyramid wavefront sensor [27] that could be integrated into rWFC. The MEMS in the PyWFS arm can be used to compensate for the static aberration seen by the PyWFS for NIRC2 operation. The CCD camera from ORKID [28], with diffraction limited observing capability could serve as valuable tool to check the optical quality of the AO bench in daytime experiments.

6.2 High order All sky Keck Adaptive optics (HAKA)

The DM actuator spacing defines the upper cutoff spatial frequency of the AO correction. A project to upgrade the Keck II AO system deformable mirror, namely, HAKA is at the early stages of development. The project consists of two parts: (1) A 3000-actuator deformable mirror (DM), replacing the existing 349-actuator DM, to reduce fitting error and enable extreme-AO performance for targets near bright natural guide stars (NGS). (2) A near-infrared tip-tilt-focus and truth sensor for laser guide star (LGS) AO to increase sky coverage and improve LGS AO performance.

For bright natural guide star (NGS) targets, atmospheric fitting error is the dominant error term in the current Keck AO system. Fitting error, along with the aliasing error and static aberrations in the system, would be reduced by increasing the number of deformable mirror (DM) actuators. Replacing the existing Keck II DM (7 mm actuator spacing), with a high-order DM (HODM; 2.5 mm actuator spacing), would reduce the residual wavefront errors of the K2 AO system by over 100 nm.

The HODM and near-infrared truth sensor (NIRT) upgrades will improve the system's performance for all currently accessible science cases while also expanding the science reach of the system. The NIRT will replace the existing low-bandwidth wavefront sensor to measure the variability in the Na layer distance and structure; the reduction in wavefront error will improve the Strehl ratio and sky coverage for LGS targets. The HODM, particularly when coupled with the ongoing real-time controller (RTC) upgrade, will enable extreme-AO-like performance for NGS targets and extend the science reach of Keck AO by enabling near diffraction-limited performance at visible wavelengths.

The Shack-Hartmann wavefront sensor pupil relay optics will be redesigned to produce a 2.8× larger pupil image on the lenslet array. The existing lenslet arrays, and reducer optics in front of the OCAM2K camera, are large enough to utilize the larger pupil. The field stop to lenslet array distance will be increased with fold mirrors. Instead of using 20 subapertures we will use 56 subapertures; a total of 224 pixels across the 240 pixel EMCCD detector.

Keck's implementation of a near-infrared pyramid sensor for low order sensing was driven by (1) NGS generally being brighter in the near-infrared (especially true for HAKA's key science targets), (2) the performance advantages of pyramid sensing, especially in the infrared where the NGS are AO-corrected, and (3) the availability of low noise detectors. Two new versions of the pupil imaging lens will be provided: one for oversampling the new DM and one to provide the low order modes for LGS AO. The former requires ≥ 55 pixels for 20 cm sampling of the Keck pupil; 63 pixels will be used due to the current pupil separation of 64.8 pixels, which still fits within a 128×128 pixel subarray on the Saphira electron avalanche photodiode detector. The latter will only be ~ 5 pixels to measure tip-tilt, focus and astigmatism. A motorized mechanism will be provided to switch between the two modes.

The HAKA upgrades will improve the performance for all current science cases while expanding the system's science reach. The HODM system will enable extreme-AO-like performance for NGS targets, including diffraction-limited

performance at visible wavelengths (with as much as 4× higher resolution than *HST*) while the near-infrared low order pyramid wavefront sensor will improve LGS AO performance and sky coverage.

7. SUMMARY

To bridge the gap between (a) the first-generation segmented telescopes and their AO systems, and (b) the next-generation telescopes and AO systems, we identified various optical and calibration effects that negatively impact the performance of the Keck telescope and the AO system, and their contributions in terms of wavefront aberration was estimated.

We propose developing a new subsystem, a residual wavefront controller (rWFC) to monitor the performance of the AO system and the environment and make necessary changes to minimize the wavefront residuals. The first results from compensating the residual segment piston errors of the Keck II telescope using the science imager, NIRC2 was presented. A summary of the expected performance improvements in terms of wavefront aberration through the rWFC is given in Table 3 for the Keck I SHWFS-OSIRIS and Keck II SHWFS NIRC2 configurations. The Keck I SHWFS-OSIRIS-TRICK would have a larger wavefront error than the Keck I SHWFS-OSIRIS.

Table 3: Summary of the expected performance improvements in terms of nm rms reduction in wavefront error through the proposed rWFC in the Keck I SHWFS-OSIRIS and Keck II SHWFS-NIRC2 configurations.

Reduction in the RMS residual wavefront errors (nm)																		
	Effect	K1 SHWFS-OSIRIS									K2 SHWFS-NIRC2							
		Seeing: 0.3"			Seeing: 0.6"			Seeing: 1"			Seeing: 0.3"			Seeing: 0.6"			Seeing: 1"	
		Zenith distance (deg.)									Zenith distance (deg.)							
		5	35	65	5	35	65	5	35	65	5	35	65	5	35	65	5	35	65
1	Spot size change due to seeing	60	60	60	25	25	25	49	49	49	22	22	22	9	9	9	18	18	18
2	Spot elongation due dispersion	1	69	401	1	69	401	1	69	401	0	23	133	0	23	133	0	23	133
3	Sub-aperture-dependent spot size/elongation	59	59	59	22	22	22	9	9	9	33	33	33	16	16	16	7	7	7
4	Random segment piston correctio	92	92	92	92	92	92	92	92	92	92	92	92	92	92	92	92	92	92
	Total RMS wavefront error (nm)	125	142	420	98	120	413	105	125	414	100	103	167	94	97	163	94	97	163

The proposed rWFC would improve the AO performance by reducing the residual wavefront aberrations. At 35 zenith distance for 0.6” seeing, the expected reduction in the RMS wavefront error is 120 nm and 97 nm for the Keck I and II AO systems, respectively.

8. ACKNOWLEDGEMENTS

The W. M. Keck Observatory is operated as a scientific partnership among the California Institute of Technology, the University of California, and the National Aeronautics and Space Administration. The Observatory was made possible by the generous financial support of the W. M. Keck Foundation. The authors wish to recognize and acknowledge the very significant cultural role and reverence that the summit of Maunakea has always had within the indigenous Hawaiian community. We are most fortunate to have the opportunity to conduct observations from this mountain.

REFERENCES

[1] Wizinowich, P., Acton, D.S., Shelton, C., Stomski, P., Gathright, J., Ho, K., Lupton, W., Tsubota, K., Lai, O., Max, C., Brase, J., An, J., Avicola, K., Olivier, S., Gavel, D., Macintosh, B., Ghez, A., Larkin, J. “First Light Adaptive Optics Images from the Keck II Telescope: A New Era of High Angular Resolution Imagery.” PASP 112, 315-319 (2000).

[2] Wizinowich, P., Le Mignant, D., Bouchez, A., Campbell, R., Chin, J., Contos, A., van Dam, M., Hartman, S., Johansson, E., Lafon, R., Lewis, H., Stomski, P., Summers, D., Brown, C., Danforth, P., Max, C., Pennington, D. “The W. M. Keck Observatory Laser Guide Star Adaptive Optics System: Overview.” PASP 118: 297-309 (2006).

[3] Ragland, S., Dupuy, T. J., Jolissaint, L., Wizinowich, P. L., Lu, J. R. et al., “Status of point spread function determination for Keck adaptive optics.”, Proc. of SPIE, 10703E, 1JR (2018).

[4] Ragland, S., “A novel technique to measure residual systematic segment piston errors of large aperture optical telescopes.”, Proc. of SPIE, 10700E, 1DR (2018).

[5] Nelson, J., American Scientist, 77, 170 (1989).

[6] Chanan, G., Troy, M., Dekens, F., Michaels, S., Nelson, J., Mast, T., Kirkman, D., Applied Optics, 37,140 (1998).

[7] Chanan, G., Ohara, C., Troy, M., Applied Optics, 39, 4706 (2000).
[8] Jia, S., et al. The Galactic Center: Improved Relative Astrometry for Velocities, Accelerations and Orbits near the Supermassive Black Hole. ApJ 873, 9J (2019).
[9] Do, T., Hees, A., Ghez, A., Martinez, G., Chu, D., Jia, S., Lu, J., Gautam, A., O'Neil, K., Becklin, E. , Morris, M., Nishiyama, S., Campbell, R., Chappell, S., Chen, Z., Ciurlo, A., Dehgganfar, A., Gallego-Cano, E., Kerzenddorf, W., Lyke, J., Naoz, S., Saida, H., Schodel, R., Takahashi, M., Takamori, Y. , Witzel, G., Wizinowich P., "Relativistic redshift of the star S0-2 orbiting the Galactic center supermassive black hole," Science 365, 664-668 (2019).
[10] Chin, J.C.Y., Cetre, S., Wizinowich, P., Lilley, S., Ragland, S., Wetherell, E., Lyke, J., Surendran, A., Correia, C., Roberto Biasi, R., Pescoller, D., Pataunar, C., Glazebrook, K., Jameson, A., Gauvin, W., Rigaut, F., Gratadour, D., Bernard, J., Delorme, J.-R., Marin, E., "Keck adaptive optics facility: real time controller upgrade,", SPIE Proc. 12185-30 (2022; this conference).
[11] Wizinowich, P., Cetre, S., Chin, J., Correia, C., Delorme, J.-R., Gers, L., Lilley, S., Lu, J., Lyke, J., Marin, E., ., Ragland, S., Richards, P.,, Surendran, A., Wetherell, E., Ghez, A., Chen, G. C.-F., Cgu, D., Do, T., Freeman, M., Gautam, A., Hunter, L., Jones, T., Liu, M., Mawet, D., Max, C., Morris, M., Terry, S., Treu, T., Wright, S. Keck All Sky Precision Adaptive Optics. SPIE Proc. 12185-25 (2022; this conference).
[12] Chu, D., Do, T., Lu, J., Gautam, A.K., Ciurlo, A., et al., "Evaluating the performance of the Keck Observatory adaptive optics systems on crowded field data using different adaptive optics configurations" (2022).
[13] Rampy, R., Femenia, B., Lyke, J., Wizinowich, P., Cetre, S., et al., "Near-infrared tip-tilt sensing at Keck: System architecture and on-sky performance" AO4ELT4, E28R (2015).
[14] Mugnier, L. M.; Sauvage, J.-F.; Fusco, T.; Cornia, A.; Dandy, S., "On-Line Long-Exposure Phase Diversity: a Powerful Tool for Sensing Quasi-Static Aberrations of Extreme Adaptive Optics Imaging Systems," Optics Express 16, 18406 (2008).
[15] Jolissaint, L., Ragland, S., Wizinowich, P., "Adaptive Optics Point Spread Function Reconstruction at W.M. Keck Observatory in Laser & Natural Guide Star Modes: Final Developments," Proc. AO4ELT4 (2016).
[16] Ragland, S., Dupuy, T.J., Jolissaint, J., Wizinowich, P.L., Lu, J.R., van Dam, M.A., Berriman, G.B., Best, W., Gelino, C.R., Ghez, A.M., Liu, M.C., Mader, J.A., Vayner, A., Witzel, G., Wright, S.A., Proc. of. SPIE (2018).
[17] Ragland, S., "A Phase Retrieval Technique to Measure and Correct Residual Segment Piston Errors of Large Aperture Optical Telescopes," Proc. of SPIE, 12182-8 (2022).
[18] Por, E. H., Haffert, S. Y., Radhakrishnan, V. M., Doelman, D. S., van Kooten, M., and Bos, S. P., "High Contrast Imaging for Python (HCIPy): an open-source adaptive optics and coronagraph simulator", in Adaptive Optics Systems VI, 2018, vol. 10703. doi:10.1117/12.2314407.
[19] Rebecca Jensen-Clem, Charlotte Z. Bond, Sylvain Cetre, Eden McEwen, Peter Wizinowich, Sam Ragland, Dimitri Mawet, James Graham, "Demonstrating predictive wavefront control with the Keck II near-infrared pyramid wavefront sensor," Proc. SPIE 11117, Techniques and Instrumentation for Detection of Exoplanets IX, 111170W (9 September 2019); https://doi.org/10.1117/12.2529687.
[20] Ciurlo, A., et al., AIROPA II: Modeling Instrumental Aberrations for Off-Axis Point Spread Functions in Adaptive Optics," JATIS (submitted, 2022).
[21] Bottom, M., Femenia, B., Huby, E., Mawet, D., Dekany, R. et al., "Speckle nulling wavefront control for Palomar and Keck.", Proc. of SPIE, 9909E, 55B (2016).
[22] Bos, S.P., Bottom, M., Ragland, S., Delorme, J.-R., Cetre, S. & Pueyo, L., "Fast and furious focal-plane wavefront sensing at W.M. Keck Observatory", Proc. of SPIE 118231E (2021).
[23] van Kooten, M.A.M, Jensen-Clem, R., Cetre, S., Ragland, S., Bond, C. Z., Fowler, J., and Wizinowich, P., "Predictive wavefront control on Keck II adaptive optics bench: on-sky coronagraphic result", *Journal of Astronomical Telescopes, Instruments, and Systems* (2022; in press).
[24] Delorme, J.-R., Jovanovic, N, Echeverri, D., Mawet, D., Wallace, J. et al, "The Keck Planet Imager and Characterizer: A dedicated single-mode fiber injection unit for high resolution exoplanet spectroscopy", submitted to JATIS (2020)
[25] van Kooten, M.A.M, Ragland, S., Jensen-Clem, R., Xin, Y., Delorme, J.-R., and Wallace, J.K., *Astrophysical Journal,* (2022; in press).
[26] Jovanovic, N., Calvin, B., Porter, M., Schofield, T. Wang, J. et al., "Enhanced high-dispersion coronagraphy with KPIC phase II: design, assembly and status of sub-modules", Proc. of SPIE, 114474U (2020).
[27] Bond, C.Z., Cetre, S., Lilley, S., Wizinowich, P., Mawet, D. et al., "Adaptive optics with an infrared pyramid wavefront sensor at Keck", JATIS, 6c9003B (2020).
[28] Peretz, E., Wizinowich, P., Lilley, S., Millar-Blanchaer, M., Kurczynski, P., et al., "ORCAS - Keck Instrument Development - ORKID", 12184-235 (2022; this conference).